Simple Model for Continuum Emission of a Protoplanetary Disk

Rosario Cecilio-Flores-Elie

May 24, 2024

Contents

1 Introduction

The evolution of protoplanetary disks is a critical process in the formation of planetary systems. These systems encompass a series of stages from their initial formation to eventual dissipation. Protoplanetary disks originate from the collapse of dense regions within molecular clouds, leading to the birth of a protostar or a young star surrounded by a rotating disk of gas and dust. This material is then held in orbit by the star's gravitational pull. The evolution and formation of these disks are due to the conservation of angular momentum, causing the material to flatten into a disk shape around the young star. These disks are rich in molecular hydrogen, small dust grains, ices, and other organic matter, setting the stage for the formation of planets.

As protoplanetary disks evolve, they undergo significant physical and chemical transformations. Over time, dust particles within the disk collide and stick together, forming larger clusters and eventually planetesimals or the building blocks of planets. Gas in disks plays a crucial role in the formation of gas giants while also being dispersed by stellar winds, radiation, and accretion on the central star. Observations of disks at various stages of evolution, from young, gas-rich disks to older, debris-filled, provide insights into the mechanisms driving these changes. Through observations, theoretical modeling, and simulations, scientists aim to understand the intricacies that govern the evolution of protoplanetary disks and the birth of planetary systems.

In this paper, we will review some models around the dust concentration, the global evolution of the dust surface density profile, and the upper limit of the grain size distribution in protoplanetary disks. (§2) Then, we will build upon the model inspired by Dr. Aleksandra Kuznetsova course *Star and Planet Formation* (§3), where a simplified model was created to show the continuum emission from a protoplanetary disk. The disk is assumed to be axisymmetric with temperature and surface density described by radial

power-law profiles. Finally, we'll look to the future of disk observations with the James Webb Space Telescope (JSWT), Nancy Grace Roman Space Telescope, and European Extremely Large Telescope (ELT) (§4) and how they will enhance our comprehension of stars and planets formation framework, as well as the additional theoretical research required to develop more comprehensive models of disk structure and evolution.

2 Protoplanetary Disk Structure and Composition

Circumstellar disks form as a consequence of angular momentum conservation during star formation. After the star accretes most of the disk material, the accretion rate decreases, leaving behind a smaller amount of material that becomes the protoplanetary disk. Throughout this process, dust plays a crucial role in the evolution, structure, and observation of these disks. Dust forms terrestrial planets and the cores of giant planets, dominates opacity, and determines the temperature structure and observational appearance of the disks.

Disk masses are best determined from submillimeter wavelength observations of dust. The continuum is optically thick in the innermost regions where column densities are high and gradually become optically thin as you observe further away from the center. The optical depth:

$$\tau_\nu = \int \rho \kappa_\nu ds = \kappa_\nu \Sigma \tag{1}$$

where Σ is the projected surface density. A frequently used method for determining dust opacity in disks (Beckwith et al. 1990) at millimeter wavelengths is

$$\kappa_\nu = 0.1(\frac{\nu}{10^{12} Hz})^\beta cm^2 g^{-}1 \tag{2}$$

where β represents power-law index and are related to the size distribution and composition of the dust grains. The normalization also contributes to the gas-to-dust ratio of 100 and ρ and Σ that equate to the total density.

For disk mass measurements on scales larger than 10 AU and in an optically thin emission the mass can be calculated by

$$M(gas + dust) = (\frac{F_\nu d^2}{\kappa_\nu B_\nu T}) \tag{3}$$

2.1 Massive Disks around Low-mass Stars

Haworth et al. 2020, explores the stability of massive disks around low-mass stars through radiation hydrodynamics calculation and simulation. It demonstrates that lower mass stars can sustain higher disk-to-star mass ratios without fragmentation, with passive irradiation from the host star playing a significant role in disk stability. The study provides model grids, criteria for disk stability, and implications for planetary system formation around M-dwarf stars like Trappist-1.

The study involved using SPH simulations to study the impact of self-gravity on protoplanetary dicks, considering different stellar luminosities and disk-to-star mass ratio to determine disk stability.

The primary focus of the study is the susceptibility of protoplanetary disks to the effects of self-gravity, based on star-disk properties. This includes determining the disk-to-star mass ratios necessary for maintaining axisymmetry, the nature of any spiral structures, and the likelihood of disk fragmentation. The study reveals that the disk-to-star mass ratio decreases over time (Figure 1), indicating a relative reduction in disk mass as the system evolves. These findings suggest that as the disk evolves, both its mass distribution and internal dynamics (e.g., viscosity) undergo significant changes.

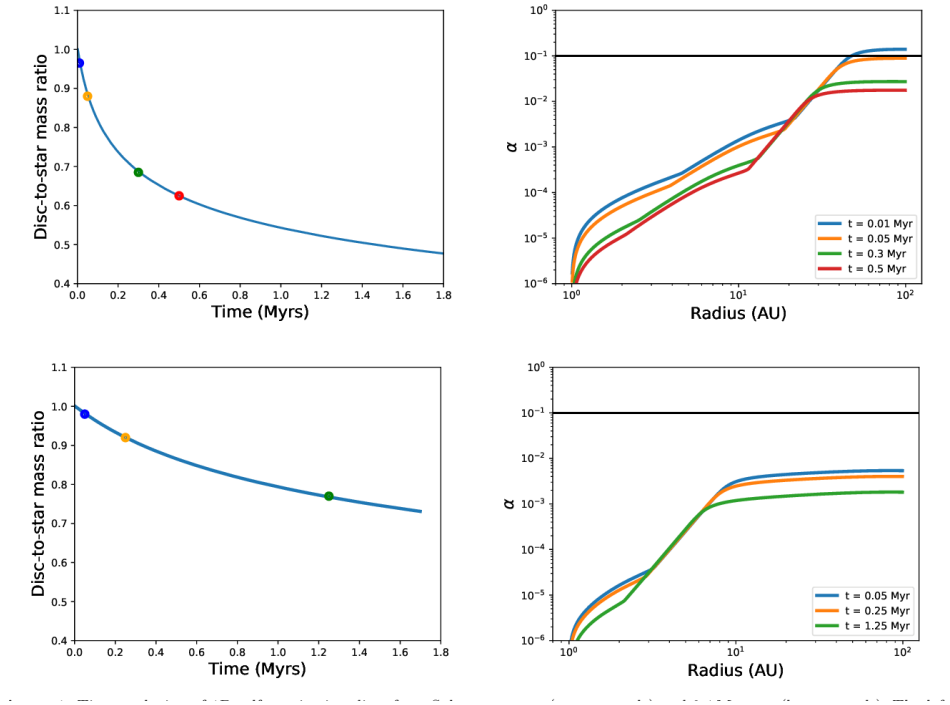

Figure 1: The time evolution of 1D self-gravitating disks is shown for a Solar mass star (top panels) and a 0.1 solar mass star (bottom panels). The left panel illustrates the disk-to-star mass ratio over time, while the right panel displays the radial effective viscous α profile at various time snapshots, marked by the points in the left panel. The horizontal black line in the right panels represents $\alpha = 0.1$, the approximate threshold above which fragmentation is expected.

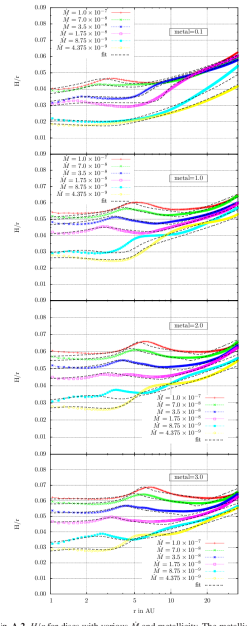

Figure 2: This series of plots shows the scale height to radius ratio (H/r) for protoplanetary discs under various conditions.

2.2 Structure of protoplanetary discs around evolving young stars

Bitsch et al. 2015, explores the evolution of protoplanetary disks and how their structure impacts planet formation. It compares simple models, such as the Minimum Mass Solar Nebula (MMSN), with more complex simulations that include viscous and stellar heating effects. The study underscores the critical importance of understanding disk structure in the context of planet formation.

The study utilizes 2D simulations of protoplanetary discs with constant accretion rates, incorporating stellar and viscous heating, and radiative cooling. The simulations are based on the magnetorotational instability (MRI) as a driver for viscosity in protoplanetary discs, focusing on the evolution of these discs over million-year timescales. One section illustrates the impact of metallicity on the disc structure, showing the variation in the aspect ratio (H/r) for discs with different mass accretion rates and metallicity levels (Figure 2).

3 Model for Dust Disk Continuum

For this project, I modified the protoplanetary disk model from Homework 10 to focus on the evolution of an M-dwarf system. The stellar parameters, including temperature, mass, and radius, were adjusted to values appropriate for an M-dwarf star. This modification allowed me to examine how these changes impact the disk properties and the resulting spectral energy distribution (SED).

3.1 Slab Model for an M-dwarf forming star region

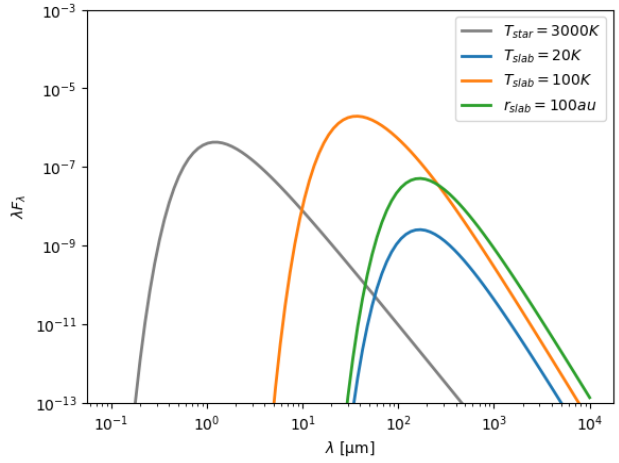

Figure 3: Slab Model for an M-Dwarf forming star system

The first plot (Figure 3) shows the spectral energy distributions (SEDs) of different components of a protoplanetary disk around a forming M-dwarf star, each characterized by their own temperature and radial position.

The gray line represents the spectral energy distribution (SED) of the central M-dwarf star, which has a temperature of 3000 K. This SED peaks in the infrared region, typical for an M-dwarf, which is cooler than solar-type stars. The curve follows the blackbody radiation profile, decreasing in intensity at longer wavelengths. The blue line represents the SED of a cooler annular slab within the disk, at a temperature of 20 K. This slab is located at a distance of 5 AU from the star and has a width of 1 AU. The peak emission is in the far-infrared region, reflecting the lower temperature of this disk region, while the intensity of emission is lower compared to the central star.

The orange line represents the SED of a warmer annular slab within the disk, at a temperature of 100 K. This slab is also located at a distance of 5 AU from the star, with a width of 1 AU. Although it peaks at shorter wavelengths compared to the blue line, indicating a higher temperature, the emission is more intense than the 20 K slab but still lower than the central star's emission. Finally, the green line represents the SED of an annular slab located farther from the star, at 100 AU. This slab also has a temperature of 20 K and a width of 1 AU. The peak wavelength is similar to the blue line since both slabs are the same temperature. However, the intensity of emission is lower due to the greater distance from the star, which affects the flux received at a given distance.

3.2 Surface Density and Temperature Profiles

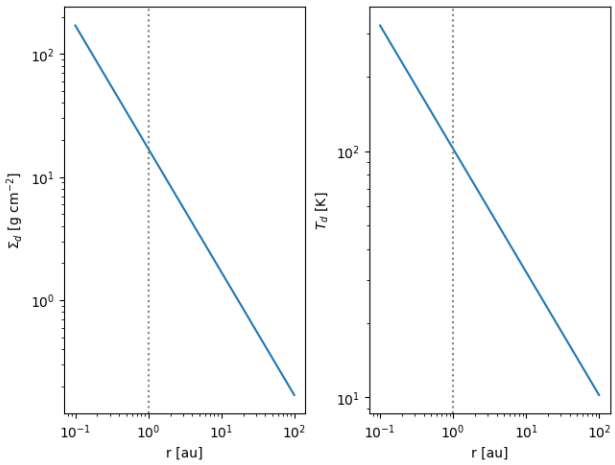

Figure 4: Density and Temperature Profiles - (Left) Surface density of dust in the disk (y-axis) and radial distance from the central star in astronomical units (AU) (x-axis), (Right) Temperature of the dust in the disk (y-axis) and the radial distance from the central star in au (x-axis)

The plot below (Figure 4) consists of two panels, each showing the radial profiles of surface density (Σ_d) and temperature (T_d) for a protoplanetary disk around an M-dwarf star. The surface density (Σ_d) decreases with increasing radius from the star, following the power-law profile.

The line follows the profile:

$$\Sigma_d(r) = \frac{\Sigma_g, 0}{g2d}(\frac{r}{r_0})^- p \tag{4}$$

where $\Sigma_g, 0$ = 1700 g cm^{-2} is the initial surface density at r_0 = 1 au, $g2d$ = 100 is the gas-to dust ratio, and p = 1.0 is the power-law index. The plot shows that at r = 0.1 au, the surface density is the highest , and it decreases steadily to r = 100 au.

The right panel reveals the radial temperature profile T_d, where it reveals a decrease in temperature with increasing radius from the star, following a power-law profile.

The line follows the profile:

$$T_d(r) = T_0(\frac{r}{r_0})^- q \tag{5}$$

where T_0 is the temperature at r_0 = 1 au, q = 0.5 is the power-law index, T_{star} = 3000 K, and $R_{star} = 0.5R_\odot$. The plot also reveals the temperature is highest close to the star (r = 0.1 au) and decreases steadily to r = 100 au. Overall, these profiles provided insights into the structure of the protoplanetary disk, showing how both surface density and temperature diminish with increasing distance from the central star.

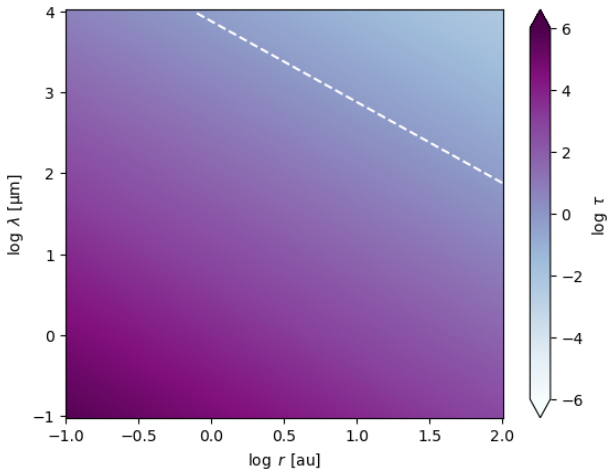

Figure 5: Heatmap - Optical Depth

3.3 Optical Depth of the Protoplanetary System

The heatmap (Figure 5) represents the optical depth (τ) of a protoplanetary disk as a function of both radial distance from the star (r) and wavelength (λ). The color scale represents the logarithm of the optical depth, while the purple region indicating lower optical depth (optically thin) and light blue region indicating higher optical depth (optically thick). The white dashed line indicates where the optical depth $\tau = 2/3$, which is a threshold used to distinguish the optically thin and optically thick regions.

As the radial distance from the star increases, the optical depth decreases. This is due to the surface density (Σ_d) of the disk decreasing with distance from the star. The decrease in optical depth with increasing radius is consistent with surface density profile:

$$\Sigma_d(r) = \frac{\Sigma_g, 0}{g2d}(\frac{r}{r_0})^- p \tag{6}$$

As the wavelength increases, the optical depth also increases. This is due to the opacity (κ_τ) of the disk material decreases with increasing wavelength. Following the power-law:

$$\kappa_\tau = \kappa_0(\frac{\lambda}{\lambda_0})^- \beta \tag{7}$$

Overall, the heatmap illustrates how the optical depth varies with both radial distance from the star and wavelength. It demonstrates that the disk is optically thick in the inner regions and at shorter wavelengths.

3.4 Spectral Energy Distribution (SED) of the Protoplanetary System

The plot below (Figure 6) displays the spectral energy distribution (SED), showing the contributions from both the star and various annuli within the disk. The gray line represents the SED of the central M-dwarf star, which has a temperature of 3000 K. The star's emission peaks in the infrared region, consistent with its cooler temperature compared to solar-type stars. The black dotted lines represent the SED contributions from individual annuli within the protoplanetary disk. These annuli are characterized by their specific temperatures and distances from the central star. The contributions from these annuli span a range of wavelengths, with each peak corresponding to the temperature of the respective annulus.

The orange line highlights the SED contributions from a particular annulus within the disk, demonstrating how a single annular region's emission contributes to the overall SED. Finally, the thick black line represents the total SED, which is the sum of the contributions from the central star and all the annuli within the disk. The total SED reflects the combined emissions from the star and the disk material.

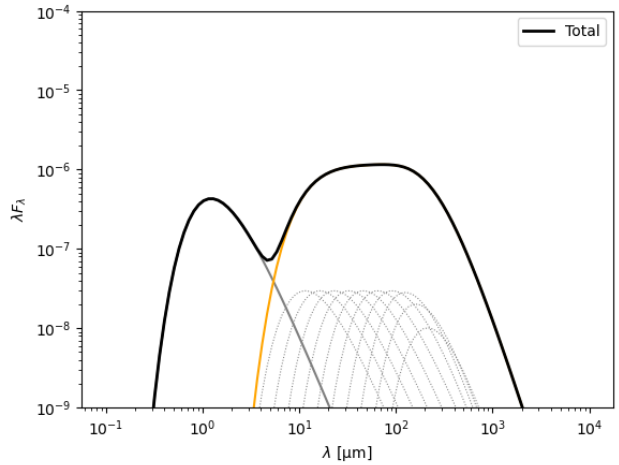

Figure 6: Spectral Energy Distribution (SED)

The SED offers a comprehensive view of the spectral energy distribution of the protoplanetary disk around an M-dwarf star, providing insight into how the central star and various regions within the disk contribute to the overall emission profile across a wide range of wavelengths.

4 Discussion and Summary

While the model provides valuable insights, there are several factors that need to be accounted for in future modeling explorations. The current model employs a simple power-law equation for dust opacity and assumes isothermal annuli, not fully capturing the complex variations in dust properties and temperature gradients within a disk. Additionally, the optically thin assumption might not hold for the denser inner regions of the disk, and the fixed properties for the central star do not consider the variability and evolution typical of young stellar objects. Comparing and contrasting this model with observational data can help close these gaps. Further improvements could include detailed radiative transfer calculations, which can account for the scattering, absorption, and re-emission of light within the disk, as well as the incorporation of grain growth and dynamic processes.

The future of observing protoplanetary disks is set to be revolutionized by the current and upcoming array of advanced observatories. The James Webb Space Telescope (JWST), which has already provided significant insights, will continue to play a pivotal role in observing the detailed structures within protoplanetary disks, such as gaps and spiral arms indicative of planet formation. Future observations with JWST will help refine our understanding of how planets interact with disk material and how these interactions shape planetary systems. Additionally, the Nancy Grace Roman Space Telescope, scheduled to launch by May 2027, will complement JWST's observations by providing further insights into these processes.

Ground-based observatories also play a crucial role in advancing our understanding of astronomical phenomena. The Atacama Large Millimeter/submillimeter Array (ALMA) and the Very Large Array (VLA) have significantly contributed to the study of protoplanetary disks, deepening our insight into planet formation processes. Modeling these disks complements observational efforts by providing a theoretical framework to interpret data and predict future observations. These models simulate the physical and chemical processes within disks, including the formation of planetary bodies and the influence of stellar radiation and magnetic fields. Ongoing and future modeling will be essential to adapt our understanding to the observations being revolutionized by JWST and upcoming observatories.

References

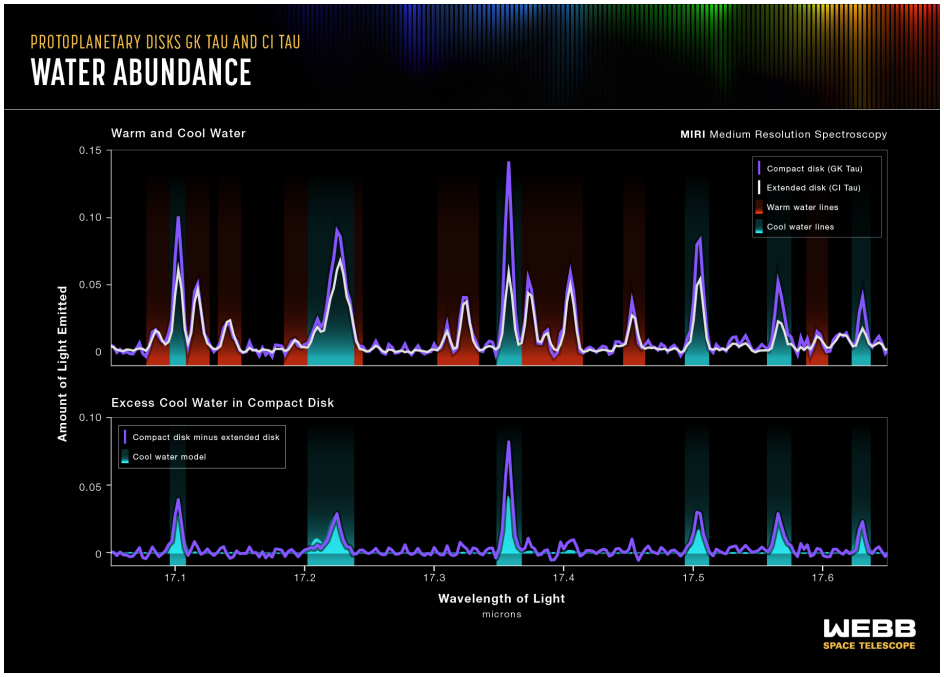

Figure 7: JWST Emission Spectrum - Water Abundance [NASA, ESA, CSA, Leah Hustak (STScI)]

Code adapted from: Dr. Aleksandra Kuznetsova. Stars & Planet Formation, 2024

Bitsch, B. *et al.* (2015) 'The structure of protoplanetary discs around evolving young stars', *Astronomy & Astrophysics*, 575, p. A28. Available at: https://doi.org/10.1051/0004-6361/201424964.

Beckwith, S.V.W. *et al.* (1990) 'A survey for circumstellar disks around young stellar objects', *The Astronomical Journal*, 99, p. 924. Available at: https://doi.org/10.1086/115385.

Backus, I. and Quinn, T. (2016) 'Fragmentation of protoplanetary disks around M-dwarfs', *Monthly Notices of the Royal Astronomical Society*, 463(3), pp. 2480–2493. Available at: https://doi.org/10.1093/mnras/stw1825.

Williams, J.P. and Cieza, L.A. (2011) 'Protoplanetary Disks and Their Evolution', *Annual Review of Astronomy and Astrophysics*, 49(1), pp. 67–117. Available at: https://doi.org/10.1146/annurev-astro-081710-102548.

Haworth, T.J. *et al.* (2020) 'Massive discs around low-mass stars', *Monthly Notices of the Royal Astronomical Society*, 494(3), pp. 4130–4148. Available at: https://doi.org/10.1093/mnras/staa883.

Fortier, A. *et al.* (2013) 'Planet formation models: the interplay with the planetesimal disc', *Astronomy & Astrophysics*, 549, p. A44. Available at: https://doi.org/10.1051/0004-6361/201220241.

Armitage, P.J. (2011) 'Dynamics of Protoplanetary Disks', *Annual Review of Astronomy and Astrophysics*, 49(1), pp. 195–236. Available at: https://doi.org/10.1146/annurev-astro-081710-102521.

Pringle, J.E. (1981) 'Accretion Discs in Astrophysics', *Annual Review of Astronomy and Astrophysics*. Annual Reviews. Available at: https://doi.org/10.1146/annurev.aa.19.090181.001033.